Mechanisms of Water Interaction with Pore Systems of Hydrochar and Pyrochar from Poplar Forestry Waste

ARTICLE *in* JOURNAL OF AGRICULTURAL AND FOOD CHEMISTRY · MAY 2014

Impact Factor: 2.91 · DOI: 10.1021/jf5010034 · Source: PubMed

6 AUTHORS, INCLUDING:

Pellegrino Conte
Università degli Studi di Palermo
132 PUBLICATIONS **2,521** CITATIONS
SEE PROFILE

Ulrich Hanke
University of Zurich
2 PUBLICATIONS **7** CITATIONS
SEE PROFILE

Valentina Marsala
Università degli Studi di Palermo
6 PUBLICATIONS **58** CITATIONS
SEE PROFILE

Giulia cimò
Università degli Studi di Palermo
8 PUBLICATIONS **23** CITATIONS
SEE PROFILE

JOURNAL OF AGRICULTURAL AND FOOD CHEMISTRY

Article

pubs.acs.org/JAFC

Mechanisms of Water Interaction with Pore Systems of Hydrochar and Pyrochar from Poplar Forestry Waste

Pellegrino Conte,*[,†] Ulrich M. Hanke,[‡,§] Valentina Marsala,[†] Giulia Cimò,[†] Giuseppe Alonzo,[†] and Bruno Glaser[‡]

[†]Dipartimento di Scienze Agrarie e Forestali, Università degli Studi di Palermo, v.le delle Scienze edificio 4, 90128 Palermo, Italy

[‡]Soil Biogeochemistry, Martin-Luther-University Halle-Wittenberg, von-Seckendorff-Platz 3, 06120 Halle, Germany

ABSTRACT: The aim of this study was to understand the water−surface interactions of two chars obtained by gasification (pyrochar) and hydrothermal carbonization (hydrochar) of a poplar biomass. The two samples revealed different chemical compositions as evidenced by solid state ^{13}C NMR spectroscopy. In fact, hydrochar resulted in a lignin-like material still containing oxygenated functionalities. Pyrochar was a polyaromatic system in which no heteronuclei were detected. After saturation with water, hydrochar and pyrochar were analyzed by fast field cycling (FFC) NMR relaxometry. Results showed that water movement in hydrochar was mainly confined in very small pores. Conversely, water movement in pyrochar led to the conclusion that a larger number of transitional and very large pores were present. These results were confirmed by porosity evaluation derived from gas adsorption. Variable-temperature FFC NMR experiments confirmed a slow-motion regime due to a preferential diffusion of water on the solid surface. Conversely, the higher number of large pores in pyrochar allowed slow movement only up to 50 °C. As the temperature was raised to 80 °C, water interactions with the pore surface became weaker, thereby allowing a three-dimensional water exchange with the bulk liquid. This paper has shown that pore size distribution was more important than chemical composition in affecting water movement in two chemically different charred systems.

KEYWORDS: *fast field cycling NMR, relaxometry, hydrochar, pyrochar, biochar, water dynamics*

INTRODUCTION

Recent scientific research addressed applications of charred biomasses for environmental remediation and agricultural productivity.[1−3] In fact, use of charred biomasses has been suggested as a solution to counteract enhancement of atmospheric carbon dioxide,[4,5] for water and soil remediation,[6−8] and for improvement of soil fertility.[2] In particular, char applied deliberately to soils, which Lehmann and Joseph[9] have recently classified as biochar, can modify soil pH,[10] increase soil draining capacity,[11] improve cation exchange capacity,[12] mitigate salt-induced stresses,[13] and interact with soil fertilizers,[14] thereby favoring microbial activity[15] and plant growth.[14,16]

Notwithstanding the positive effects of biochar applications to soils, some authors have warned about its potential detrimental impacts on the environment. For example, increase of CO_2 emissions to atmosphere, due to enhancement of soil C mineralization rate after biochar applications to soils, has been described.[17] Also, plant growth inhibition due to temporary high pH values, the presence of volatile matter (i.e., tars, resins, and other short-lived substances that remain on the biochar surface immediately after production), and nutrient imbalances associated with the use of fresh biochars has been reported.[18,19]

Certainly, functions of chars in the environment depend on their physicochemical properties, which, in turn, are most affected by feedstock type, pyrolysis conditions, and duration of charring.[3,9−11,20−25] As an example, aromatic condensation in chars increases with increasing heating temperature.[20,24] Moreover, plant species with many large-diameter cells in the stem tissues can lead toward chars containing larger amounts of macropores.[9] Macropores in biochar applied to soils may enhance soil drainage and capacity to retain large molecules such as phenolic compounds.[11] On the other hand, micropores may adsorb water with high capillary forces so that it is not available for most plants. For this reason, understanding char physical and chemical processes at the char surface is very crucial to address its agronomical and environmental uses and allow meaningful preapplication quality assessments.

Nuclear magnetic resonance (NMR) techniques are usually applied to monitor char characteristics.[10,20,22,24,26] In particular, low-field NMR relaxometry with fast field cycling setup (FFC NMR) can be used to study the dynamics of water in chars to retrieve information about the possible molecular mechanisms through which water (and therefore micro- and macronutrients) can be drained in char-amended soils.

In previous studies, FFC NMR relaxometry was applied to differentiate among pore size distribution on the surface of chars obtained by an industrial gasification procedure[10] and to recognize the nature of the interactions between water and char surfaces.[26] These studies were conducted only on chemically identical chars. However, no information is available on the dynamics of water in chars having different chemical compositions. For this reason, in the present study, we selected a hydrochar already analyzed by Wiedner et al.[24] and a pyrochar studied in De Pasquale et al.[10] and Conte et al.,[26] both obtained by the same biomass feedstock, with the aim to investigate the

Received: February 27, 2014
Revised: May 8, 2014
Accepted: May 9, 2014

   dx.doi.org/10.1021/jf5010034 | J. Agric. Food Chem. XXXX, XXX, XXX−XXX

role played by chemical characteristics on water dynamics within the pore system of the chars.

MATERIALS AND METHODS

Feedstock. The hydrochar and pyrochar samples were prepared by using poplar (*Populus* spp. L.) wood chips that were obtained from a dedicated short-rotation forest in the Po valley (Gadesco Pieve Delmona, 45°10^{I}13^{II} N, 10°06^{I}01^{II} E). The age of the forest at the time of harvest was 5 years. The characteristics of the biomass were already described in De Pasquale et al.[10]

Pyrochar and Hydrochar Preparation. Pyrochar was produced by using an industrial gasifier at the temperature of 1200 °C. All of the details about the gasifier and the pyrolitic conditions have been already reported in De Pasquale et al.[10] Hydrochar was obtained in a b.coal 2.0 reactor from Artec Biotechnology GmbH (Bad Königshofen, Germany) at 230 °C and 40 bar. Details about the procedure have been reported already in Wiedner et al.[24] Both pyrochar and hydrochar samples were 2 mm sieved with a stainless steel sieve and dried overnight in an oven set at 105 °C before each NMR analysis.

Specific Surface Area Measurement. Samples were first dried at 200 °C for 4.5 h and then stored in a desiccator. To retrieve the specific surface area by applying the Brunauer−Emmett−Teller (BET) five-point method, samples were degassed with N_2 at 200 °C for another hour and then measured in liquid N_2 (Quantachrome NOVA 4200 calibrated with BAM-PM-104) following DIN ISO 9277:2003-05. All measurements were done in triplicate. Specific surface areas of the pyrochar and the hydrochars were 54.6 ± 0.2 and 129 ± 2 $m^2\ g^{-1}$, respectively.

The poplar pyrochar surface area measured in this study was smaller than that already reported in De Pasquale et al.[10] (i.e., 98 ± 6 $m^2\ g^{-1}$). The difference can be explained by the different sample preparation used in De Pasquale et al.[10] prior to BET analysis. In fact, the BET investigations reported in De Pasquale et al.[10] have been conducted on agate−mortar ground samples. Pyrochar grinding reduces particle sizes, thereby increasing surface area values.

Evaluation of Pore Size Distribution from the Specific Surface Area Measurements. The nonlocal density functional theory (NLDFT) equilibration model[27] was applied to elaborate the isotherms (35 adsorption and 30 desorption points) of nitrogen adsorption experiments to achieve pore size distributions. Assumption of N_2 at −196 °C on carbon (slit-pore) was used. The cumulative pore volumes and surface areas for the micropore class (i.e., <2 nm, according to IUPAC classification) retrieved by the NLDFT model were 16.3 × 10^{-3} $cm^3\ g^{-1}$ and 29.4 $m^2\ g^{-1}$ for pyrochar, whereas they were 50.9 × 10^{-3} $cm^3\ g^{-1}$ and 93.3 $m^2\ g^{-1}$ for hydrochar. NLDFT surface area and pore volume for hydrochar were around 3 times higher than those for pyrochar, thereby evidencing that the number of pores in the former sample was larger than in the latter one. In particular, the surface/volume (S/V) ratios from NLDFT elaborations were $(S/V)_{pyrochar}$ = 1.80 × 10^9 m^{-1} and $(S/V)_{hydrochar}$ = 1.83 × 10^9 m^{-1}.

CP-TOSS ^{13}C NMR Spectra. Cross-polarization magic angle spinning (CPMAS) ^{13}C NMR measurements were performed on a Bruker Avance-II 400 spectrometer (Bruker Biospin, Milan, Italy) operating at 100.6 MHz on carbon-13 and equipped with a 4 mm standard-bore solid state probe. Samples were packed into 4 mm zirconia rotors with Kel-F caps, and the rotor spin rate was set at 5000 ± 2 Hz. A spectral width of 25252.52 Hz centered at 10061.78 Hz, an optimum contact time of 1 ms chosen after evaluation of variable contact time experiments, a recycle delay of 20 s, and 2K data points over an acquisition time of 35 ms were used. The spectra were acquired with the total suppression side bands (TOSS) sequence with a 50% RAMP to prevent artifacts in the spectra interpretation. A 4.1 μs ^{1}H 90° pulse with an attenuation level of −2.4 dB was applied. Spectra acquisition was achieved with Bruker Topspin 2.0. Data processing was done with MestRe-C software (version 4.9.9.9, Mestrelab Research, Santiago de Compostela, Spain). The free induction decays (FIDs) were transformed by applying first a 2K zero filling, then a line broadening of 100 Hz, and finally an automatic baseline correction with a third-order polynomial and Bernstein algorithm.

Fast Field Cycling (FFC) NMR Relaxometry. The 2 mm sieved and dried poplar pyrochar and hydrochar samples have been prepared as slurry for FFC NMR relaxometry investigations according to the procedure reported in Dunn et al.[28] The background theory of FFC NMR relaxometry has been already described in De Pasquale et al.[10] Moreover, more general environmental applications of FFC NMR relaxometry can be found in Conte and Alonzo.[29]

^{1}H NMR dispersion profiles (i.e., relaxation rates R_1 or $1/T_1$ vs proton Larmor frequencies) were acquired on a Stelar Spinmaster FFC2000 Relaxometer (Stelar s.r.l., Mede, PV, Italy) at temperatures of 25, 50, and 80 °C. The proton spins were polarized at a B_{POL} corresponding to the proton Larmor frequency (ω_L) of 24 MHz for a T_{POL} corresponding to about 5 times the T_1 estimated at this frequency. After each B_{POL} application, the magnetic field intensity (indicated as B_{RLX}) was systematically changed in the proton Larmor frequency ω_L comprised in the range 0.01−40 MHz. The period τ, during which B_{RLX} was applied, has been varied on 32 logarithmic spaced time sets, each of them adjusted at every relaxation field to optimize the sampling of the decay/recovery curves. FIDs were recorded following a single ^{1}H 90° pulse applied at B_{ACQ} corresponding to the proton Larmor frequency of 16 MHz. A time domain of 100 μs sampled with 512 points was applied. Field switching time was 3 ms, whereas spectrometer dead time was 15 μs. For all experiments, a recycle delay of 12 s was used. The NP sequence was applied when the relaxation magnetic fields were in the range of the proton Larmor frequencies between 40.0 and 9.0 MHz. The PP sequence was applied in the proton Larmor frequencies B_{RLX} range of 9.0−0.01 MHz.[30]

FFC NMR Data Processing. R_1 values were achieved by interpolating the ^{1}H magnetization decay/recovery curves at each B_{RLX} value (i.e., ^{1}H signal intensity vs τ) with the stretched exponential function (also known as the Kohlrausch−Williams−Watts function) reported in eq 1 after exportation of the experimental data to OriginPro 7.5 SR6 (version 7.5885, OriginLab Corp., Northampton, MA, USA). This equation provided the best fitting with the largest coefficients of determination (R^2 > 0.998). The choice of this function was due to the large sample heterogeneity resulting in a multi-exponential behavior of the decay/recovery curves.[29,31] This approach has the advantage that it is able to handle a wide range of behaviors within a single model. For this reason, assumptions about the number of exponentials to be used in modeling NMRD data are not necessary.

$$I(\tau) = I_0 \exp[-(\tau/T_1)^k] \quad (1)$$

In eq 1, $I(\tau)$ is the ^{1}H signal intensity at each fixed B_{RLX}, I_0 is the ^{1}H signal intensity at the thermal equilibrium, T_1 is the average proton spin−lattice relaxation time, and k is a heterogeneity parameter related to the stretching of the decay process. This function can be considered as a superposition of exponential contributions, thereby describing the likely physical picture of some distribution in T_1.

Relaxation data at the proton Larmor frequency of 40 MHz were evaluated by the inverse Laplace transformation through application of the UPEN algorithm (Alma Mater Studiorum, Università di Bologna, Italy)[32,33] with the aim to obtain the T_1 distributions at such magnetic field and, therefore, information on pore distribution and grain size. The choice of UPEN analyses only at 40 MHz was due to the larger NMR sensitivity at this frequency as compared to the other proton Larmor frequencies.[30]

RESULTS AND DISCUSSION

Hydrochar and Pyrochar Chemical Composition by CP-TOSS ^{13}C NMR Spectroscopy. The cross-polarization magic angle spinning with total suppression of side bands ^{13}C NMR spectra of the two samples studied here showed the more complex nature of hydrochar as compared to pyrochar (Figure 1). In particular, two main regions can be recognized in the hydrochar spectrum (Figure 1A). The first chemical shift

dx.doi.org/10.1021/jf5010034 | J. Agric. Food Chem. XXXX, XXX, XXX−XXX

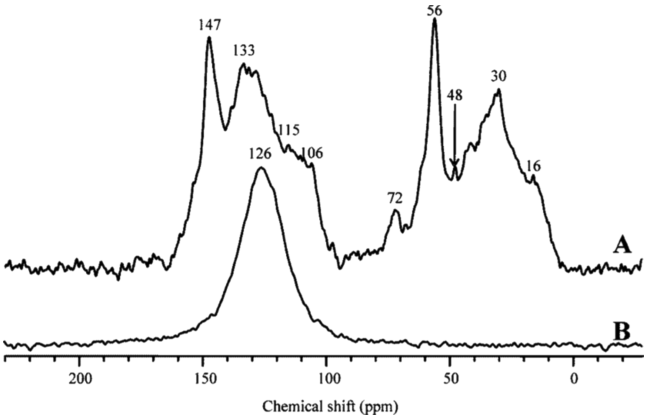

Figure 1. CP-TOSS ^{13}C NMR spectra of poplar hydrochar (A) and pyrochar (B).

interval between 0 and 80 ppm contains individual signals at 16, 30, 48, 56, and 72 ppm (Figure 1A). The first signal at 16 ppm can be attributed to methyl groups of terminating alkyl chains; the second one at 30 ppm is due to methylene groups in alkyl chains, whereas the signal at 48 ppm can be assigned to branched alkyl carbons; the signal at 56 ppm is assignable to methoxyl groups in lignin-like structures, and that at 72 ppm is due to carbons C2, C3, and C5 in the residual cellulose moiety from the poplar biomass.[24,34]

The second spectral region in Figure 1A occurred in the chemical shift interval between 90 and 160 ppm. The main signals recognized in this region are broad bands centered at 106, 115, 133, and 147 ppm. The signal at 106 ppm can be assigned to C1 in residual cellulose; that at 115 ppm is due to C5 in guaiacyl (G) and C3 and C6 in *p*-hydroxyphenyl groups; the signal at 133 ppm is due to the aromatic C−5/C−5′ in etherified 5−5 G units; finally, the signal at 147 ppm is assigned to C3 and C4 in etherified guaiacyl units.[24,34]

The spectrum reported in Figure 1B reveals only one broad band at 126 ppm, which can be assigned to polyaromatic systems.[10] The differences in the chemical composition of poplar hydrochar and pyrochar samples (Figure 1) can be explained by the different types of reactions occurring as either hydrothermal carbonization[24] or gasification[10] is applied. The hydrothermal carbonization used in this study consisted of a thermal degradation of the water-suspended biomass at high pressure and 230 °C by applying citric acid as catalyst.[24] During this process, carbohydrates in poplar biomass have been gradually transformed to aromatic and aliphatic structures, thereby providing a lignin-like material. However, the presence of signals at 56, 72, 106, 133, and 147 ppm (Figure 1A) indicates that the hydrothermal carbonization produced a carbonaceous material still containing oxygenated functionalities, but almost no polycondensed aromatic moieties as outlined in Wiedner et al.[24]

The sole aromatic signal in the CP-TOSS ^{13}C NMR spectrum of the poplar pyrochar (Figure 1B) is due to the diamagnetic currents produced by delocalized π-electrons in extended aromatic structures or graphite-like microcrystallites, which are generated by the high-temperature condensations as biomass feedstock is subjected to gasification.[10]

Effect of Pore Size on ^1H NMR T_1 Distributions. The 2 mm sieved poplar hydrochar and pyrochar samples were saturated with water and the slurry was analyzed by fast field cycling NMR relaxometry as indicated under Materials and Methods. Figure 2 reports the distributions of the longitudinal relaxation times (T_1), also referred to as relaxograms, at the

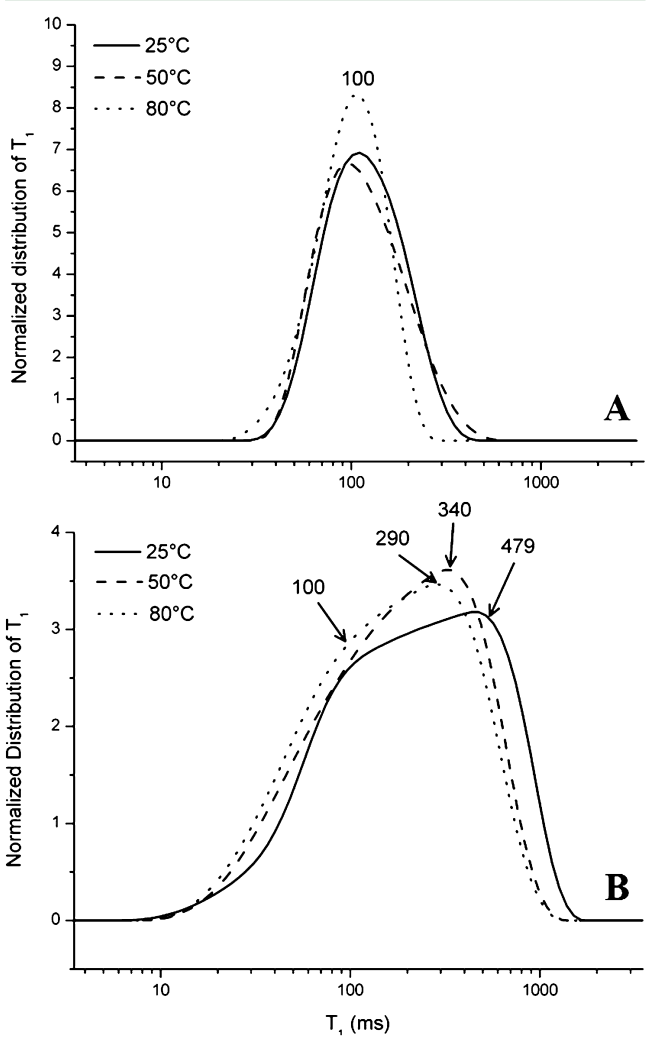

Figure 2. Relaxograms of poplar hydrochar (A) and pyrochar (B) acquired at the proton Larmor frequency of 40 MHz.

proton Larmor frequency of 40 MHz and three temperatures (25, 50, and 80 °C) as obtained by applying the inverse Laplace transformation of the relaxation data through the UPEN algorithm (see Materials and Methods).

Proton longitudinal relaxation times of water in porous media are affected by the collisions between the liquid state molecules and the walls of the porous boundaries.[35] In particular, longitudinal relaxation is dominated by the presence of a strong relaxation sink at the pore surface, which is imputable to the temporary adsorption of water on the solid surface.[36] Temporary adsorption can be achieved by formation of weak unconventional hydrogen bonds on the surface of pyrogenic char systems as already outlined in Conte et al.[26] and Conte and Alonzo.[29] However, as surficial polar groups are present, the weak unconventional H-bonds may turn toward stronger conventional ones, which may hook water molecules more strongly on the char surface. The effectiveness of the aforementioned relaxation sink depends on the ratio between the pore surface and the pore volume as well as on the diffusion rate across the pore.[37] In fact, space restriction in small-sized pores does not allow fast molecular mobility. As this condition

dx.doi.org/10.1021/jf5010034 | J. Agric. Food Chem. XXXX, XXX, XXX−XXX

occurs, $^1H-^1H$ dipolar interactions become very efficient. Shorter relaxation times are, hence, retrieved.[35,37,38] Conversely, as pore size enlarges, molecular mobility increases and strength of dipolar interactions weakens. For this reason, longer relaxation times are expected.[35,37,38] As the number and size of the various pores present in a material is heterogeneous, water must diffuse through the differently sized pores, thereby providing a wide ensemble of longitudinal relaxation times that appear continuously distributed. The lowest limit of such an ensemble (the shortest T_1 value) is due to water moving into the smallest pores, whereas the highest limit (the longest T_1 value) is attributed to water moving into the largest pores. All T_1 values between the two limits are due to the dynamics of water inside pores having sizes lying between the two extremes.[29] According to the aforementioned mechanism, the differences observed at the same temperatures between the T_1 distributions reported in Figure 2 can be attributed to different pore size distributions present in the hydrochar and pyrochar samples. In particular, a homogeneous distribution of small-sized pores can be recognized in hydrochar rather than in pyrochar. The latter, in turn, is made by a less homogeneous distribution of pores, which are on average larger than in hydrochar. In fact, all of the hydrochar relaxograms showed a maximum centered at a T_1 value of around 100 ms regardless of the temperature used during the experiments (Figure 2A). Conversely, the relaxograms acquired for the water-saturated pyrochar span a larger interval of T_1 values (Figure 2B). Here a maximum at 100 ms independent of the applied temperature (similarly to the water-saturated hydrochar sample) can be observed. Moreover, second maxima centered at 479, 340, and 290 ms retrieved at 25, 50, and 80 °C, respectively, are also observed (Figure 2B). A wide distribution of T_1 values is included among the two longitudinal relaxation time limits in Figure 2B. We can identify water molecules relaxing at 100 ms in both carbonaceous samples as those restricted in the smallest sized pores; water molecules generating the maxima at 479 ms at 25 °C, 340 ms at 50 °C, and 290 ms at 80 °C as those tumbling in the largest pores; and, finally, water molecules relaxing in the intervals of 100−479 ms at 25 °C, 100−340 ms at 50 °C, and 100−290 ms at 80 °C as those occluded in transitional pores.

The aforementioned findings are supported by BET and NLDFT elaborations as reported under Materials and Methods. In fact, specific surface areas were 54.6 ± 0.2 and 129 ± 2 m^2 g^{-1} for pyrochar and hydrochar, respectively, thereby suggesting a larger volume of pores in the former than in the latter sample. On the other hand, NLDFT elaborations of isotherms obtained from nitrogen adsorption provided S/V ratios in the order $(S/V)_{pyrochar} < (S/V)_{hydrochar}$ (see Materials and Methods). It is well-known that the longitudinal relaxation rate $(1/T_1)$ is directly proportional to the S/V ratio[39] or by considering the reciprocal:

$$T_1 \propto \frac{V}{S}$$

Because $(S/V)_{pyrochar} < (S/V)_{hydrochar}$, it happens that $(V/S)_{pyrochar} > (V/S)_{hydrochar}$ and it is expected that the T_1 values for pyrochar must be longer than for hydrochar. The latter expectation has been evidenced in the experimental results shown in Figure 2 and discussed above.

It is interesting to note that the relaxogram reported in De Pasquale et al.[10] was obtained for the same pyrochar used in the present study. However, the T_1 distribution in De Pasquale et al.[10] revealed a larger pore size homogeneity than the relaxogram reported here in Figure 2B. This difference can be explained by considering that samples were prepared differently prior to the analysis. In fact, in the present study, we sieved the poplar pyrochar at <2 mm, whereas in De Pasquale et al.[10] the sample has been ground. As already outlined under Materials and Methods, sample grinding reduces pore size, thereby allowing larger surface area and more homogeneous pore size distribution.

Effect of Temperature on ^1H NMR T_1 Distributions. Longitudinal relaxation times are dependent not only on the pore size distribution, as outlined in the previous paragraph, but also on temperature variations.[29] In fact, it is well recognized that temperature increments accelerate molecular motions, thereby weakening the $^1H-^1H$ dipolar interactions responsible for the longitudinal relaxation of a liquid moving on the surface of porous materials.[40] When this condition occurs, an increase of T_1 values is expected because a longer time is needed for proton spin−lattice relaxation. However, it has been already shown that water retained in charred materials behaves diametrically, thereby suggesting that water dynamics is subjected to a slow-motion regime.[26] The latter is achieved when water molecules are hooked to the char surface via weak hydrogen bonds that may arise by the overlay of the electron-deficient orbitals of protons in water and the electron-rich orbitals in the organic and inorganic components of the charred system.[26] As temperature increases, the weak interactions, which allow water adhesion to the pore walls, oppose the 3D exchange with the bulk water (i.e., the replacement of water molecules hooked to the char surface with those appertaining to the bulk liquid).[40] For this reason, water preferentially diffuses more quickly within the channels connecting pores between one another through a two-dimensional (2D) motion (i.e., the diffusion of water molecules within the channels connecting either different surface pores or char surface with the interior part of the same material).[26,40] Due to the 2D surface diffusion just described, the water collision frequency with pore walls increases with temperature, thereby allowing an average residence time on pore walls longer than that retrieved at lower temperatures. Because of this, a shorter time for protons to relax is needed and lower T_1 values are achieved.[40] As a consequence, relaxograms, such as those in Figure 2, shrink as the temperature is increased. Moreover, it must be added that the larger the pore size, the more pronounced is the reduction of the relaxogram width and the reduction of the T_1 maxima. In fact, upon temperature increasing, water collision frequency in larger pores becomes higher than in the more spatially restricted ones. Because of this, the average time spent by water molecules on pore walls is higher in the transitional and largest pores than in the smallest pores. The latter is why the reduction of relaxogram widths is less pronounced in Figure 2A than in Figure 2B. Moreover, the same mechanism explains why the maximum at 100 ms due to water in the smallest pores either in hydrochar or in pyrochar is unaffected by temperature changes, whereas the T_1 maxima due to water in larger sized pores (T_1 >100 ms) shift toward shorter values.

Nuclear Magnetic Resonance Dispersion (NMRD) Profiles. Figure 3 shows the NMRD profiles (i.e., $R_1 = 1/T_1$ values vs ω_L) at 25, 50, and 80 °C for the water-saturated poplar hydrochar and pyrochar samples investigated here. In particular, the NMRD profiles of the former sample are all placed at faster longitudinal relaxation rates (Figure 3A) as compared to the NMRD profiles of the latter sample (Figure

dx.doi.org/10.1021/jf5010034 | J. Agric. Food Chem. XXXX, XXX, XXX−XXX

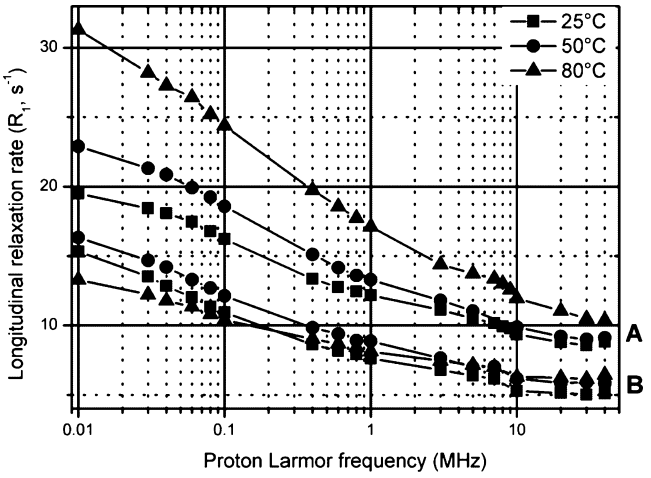

Figure 3. NMRD profiles of poplar hydrochar (A) and pyrochar (B).

3B). This is due to the differences in the surface areas between the two porous materials. In fact, $SSA_{hydrochar}$ was larger than $SSA_{pyrochar}$ (see above). The larger the surface area value, the smaller is the size of the pores. Restriction of water in small pores leads to stronger $^1H-^1H$ dipolar interactions, which, in turn, are the cause for the very efficient proton longitudinal relaxation in hydrochar (i.e., faster R_1 values) compared to pyrochar.[41]

It is worth noting that all of the NMRD profiles in Figure 3A are translated toward faster R_1 values in the whole range of proton Larmor frequencies as the temperature is increased. This behavior accords with that already described in Conte et al.,[26] thereby confirming the slow-motion regime also outlined in the previous paragraph. However, Conte et al.[26] reported that the slow-motion regime on the surface of char systems is due to nonconventional H-bonds arising by the overlay between the electron-deficient orbitals of protons in water and the electron-rich orbitals of the aromatic organic centers in the charred material. In the present study, we have reported that hydrothermal degradation did not remove all of the oxygen-containing functionalities (see above). For this reason, we cannot exclude participation of the more traditional O−H··· O bonds in the slow-motion regime observed for the hydrochar sample.

Figure 3B reveals that the NMRD profiles acquired for the pyrochar sample behaved similarly to the hydrochar only up to 50 °C. Conversely, an anomalous trend was observed at 80 °C. In fact, a slight increment of the R_1 values was retrieved between 40 and 10 MHz as the temperature was switched from 50 to 80 °C. Then the 80 °C NMRD profile crossed the one acquired at 50 °C as ω_L was set to 10 MHz and that retrieved at 25 °C as ω_L was switched to 0.2 MHz (Figure 3B). The H-bond-mediated slow-motion regime can explain the NMRD behavior up to 50 °C observed for the pyrochar sample (Figure 3B). However, as the temperature is raised to 80 °C, a chemical exchange with the bulk phase must be considered to account for the anomalous behavior reported in Figure 3B.[40]

The interesting feature that the temperature dependence of water dynamics in hydrochar is opposite than that observed in pyrochar can be explained only by considering the different pore size distribution in the two carbonaceous samples. In fact, as outlined above, the average pore size in hydrochar is smaller than in pyrochar. Water molecules are more tightly trapped in the former than in the latter material. For this reason, water can easily run toward the bulk liquid from pyrochar rather than from hydrochar surface as the temperature is increased to 80 °C.

The comparison among the temperature dependences of the NMRD profiles in Figure 3 and those in Conte et al.[26] supports the latter hypothesis on the role played by pore size in water exchange with the bulk solution. In fact, the pyrochar analyzed either in the present study or in Conte et al.[26] was obtained by the same gasification process.[10] However, whereas in Conte et al.[26] the pyrochar was ground in an agate mortar before NMRD investigations, here we have performed NMRD analyses after having sieved the same material to <2 mm. As a consequence, the surface area of the ground pyrochar[26] was larger than that used in the present study. As already noted above, larger surface area was associated with a more homogeneous pore size distribution made mainly by the smallest pores. Conversely, a more inhomogeneous distribution of pore size (with a larger contribution from transitional and larger pores) was identified in the porous charred material having a lower surface area. Hence, the more inhomogeneous pore size pyrochar used here revealed the anomalous temperature dependence behavior at 80 °C (Figure 3B) due to the higher number of larger pores, which make the exchange of surface water molecules with the bulk ones easier.

This paper reports high- and low-field NMR characterization of the physicochemical properties of hydrochar and pyrochar samples retrieved by applying either hydrothermal treatment or gasification to poplar forestry wastes. In particular, high-field NMR spectroscopy (i.e., CP-TOSS ^{13}C NMR) revealed that the thermal treatments produced two chemically different carbonaceous materials. Although poplar hydrochar appeared as a lignin-like material still containing oxygenated functionalities, poplar pyrochar emerged as a polyaromatic system where O-containing groups were not detected.

Notwithstanding the different chemical compositions, the mechanisms of water dynamics on the surface of poplar hydrochar and pyrochar were affected more by their physical characteristics rather than by their chemical peculiarities. In particular, isothermally 40 MHz acquired relaxograms revealed that water motion was more restricted in hydrochar than in pyrochar, thereby suggesting that the former sample included a larger number of small-sized pores than the latter one. On the other hand, the freer motion of water in pyrochar indicated a higher amount of transitional and very large pores.

Variable-temperature relaxometry experiments revealed that a 2D surface diffusion mechanism was the only force responsible for water motion in hydrochar up to the temperature of 80 °C. Surface diffusion was the predominating motion mechanism of water in pyrochar only up to 50 °C. Conversely, a 3D exchange with the bulk water appeared to interfere with the aforementioned 2D diffusion as the temperature was raised to 80 °C.

The differentiation between the 2D diffusion and the 3D exchange mechanisms was attributed to the different porosities in the charred materials. In fact, water constrained in small pores such as in hydrochar strongly interacts with the solid surfaces. For this reason, its fugacity toward the bulk liquid is inhibited in the whole temperature interval investigated here (25−80 °C). On the other hand, the larger pore sizes in poplar pyrochar prevent water exchange with the bulk solution only in a more restricted temperature interval (namely, 25−50 °C). As the temperature overcomes the limit of 50 °C, water surface

dx.doi.org/10.1021/jf5010034 | J. Agric. Food Chem. XXXX, XXX, XXX−XXX

interactions become weaker and 3D exchange with the bulk liquid occurs.

Although in the present study the chemical composition of poplar hydrochar and pyrochar appeared of minor importance to the water dynamics, its contribution to the strength of water solid phase interactions is not yet clear. For this reason, more detailed studies on the effect of pore sizes and chemical composition of charred materials on water dynamics are urgently needed.

AUTHOR INFORMATION

Corresponding Author

*(P.C.) E-mail: pellegrino.conte@unipa.it. Phone: 0039 09123864673. Fax: 0039 091484035.

Present Address

§(U.M.H.) Soil Science and Biogeochemistry, University of Zurich, Winterthurerstrasse 190, 8057 Zürich, Switzerland.

Funding

We appreciate the support of COST action TD1107 (Biochar for sustainable resources management) for the Short-term Scientific Mission (STSM) for U.M.H.

Notes

The authors declare no competing financial interest.

ACKNOWLEDGMENTS

We are grateful to Centro Grandi Apparecchiature − UniNetLab of Università degli Studi di Palermo (http://www.unipa.it/cga/index.html) for having provided machine time at the high-field NMR spectrometer for the acquisition of the CP-TOSS ^{13}C NMR spectra. We acknowledge Dr. Alessandro Pozzi (AGT technologies) for providing the pyrochar sample.

REFERENCES

(1) Glaser, B.; Haumaier, L.; Guggenberger, G.; Zech, W. The "Terra Petra" phenomenon a model for sustainable agriculture in the humid tropics. *Naturwissenschaften* **2001**, *88* (1), 37−41, DOI: 10.1007/s001140000193.

(2) Mao, J. D.; Johnson, R. L.; Lehmann, J.; Olk, D. C.; Neves, E. G.; Thomson, M. L.; Schmidt-Rohr, K. Abundant and stable char residues in soils: implication for soil fertility and carbon sequestration. *Environ. Sci. Technol.* **2012**, *46*, 9571−9576.

(3) Mukherjee, A.; Lal, R. Biochar impacts on soil physical properties and greenhouse gas emissions. *Agronomy* **2013**, *3* (2), 313−339, DOI: 10.3390/agronomy3020313.

(4) Glaser, B.; Lehmann, J.; Zech, W. Ameliorating physical and chemical properties of highly weathered soils in the tropics with charcoal − a review. *Biol. Fert. Soils* **2002**, *35* (4), 219−230, DOI: 10.1007/s00374-002-0466-4.

(5) Vanderslice, N. C.; Marrero, T. R. Impact of bio-char on carbon dioxide in the atmosphere. In *Proceedings of the 2009 Midwest Section Conference of the American Society for Engineering Education*, 2009; available at http://www.asee.org/papers-and-publications/papers/section-proceedings/midwest/.

(6) Mohan, D.; Rajput, S.; Singh, V. K.; Steele, P. H.; Pittman, C. U., Jr. Modeling and evaluation of chromium remediation from water using low cost bio-char, a green adsorbent. *J. Hazard. Mater.* **2011**, *188* (1−3), 319−333, DOI: 10.1016/j.jhazmat.2011.01.127.

(7) Beesley, L.; Moreno-Jiménez, E.; Gomez-Eyles, J. L.; Harris, E.; Robinson, B.; Sizmur, T. A review of biochars' potential role in the remediation, revegetation and restoration of contaminated soils. *Environ. Pollut.* **2011**, *159* (12), 3269−3282, DOI: 10.1016/j.envpol.2011.07.023.

(8) Zhang, X.; Wang, H.; He, L.; Lu, K.; Sarmah, A.; Li, J.; Bolan, N. S.; Pei, J.; Huang, H. Using biochar for remediation of soils contaminated with heavy metals and organic pollutants. *Environ. Sci. Pollut. Res.* **2013**, *20* (12), DOI: 10.1007/s11356-013-1659-0.

(9) Lehmann, J.; Joseph, S. Biochar for environmental management: an introduction. In *Biochar for Environmental Management: Science and Technology*; Lehmann, J., Joseph, S., Eds.; Routledge: London, UK, 2009; pp 448.

(10) De Pasquale, C.; Marsala, V.; Berns, A. E.; Valagussa, M.; Pozzi, A.; Alonzo, G.; Conte, P. Fast field cycling NMR relaxometry characterization of biochars obtained from an industrial thermochemical process. *J. Soils Sediments* **2012**, *12* (8), 1211−1221, DOI: 10.1007/s11368-012-0489-x.

(11) Warnock, D. D.; Lehmann, J.; Kuyper, T. W.; Rilling, M. C. Mycorrhizal responses to biochar in soil − concepts and mechanisms. *Plant Soil* **2007**, *300* (1−2), 9−20, DOI: 10.1007/s11104-007-9391-5.

(12) Liang, B.; Lehmann, J.; Solomon, D.; Kinyangi, J.; Grossman, J.; O'Neill, B.; Skjemstad, J. O.; Thies, J.; Luizão, F. J.; Petersen, J.; Neves, E. G. Black carbon increases cation exchange capacity in soils. *Soil Sci. Soc. Am. J.* **2006**, *70* (5), 1719−1730, DOI: 10.2136/sssaj2005.0383.

(13) Thomas, S. C.; Frye, S.; Gale, N.; Garmon, M.; Launchbury, R.; Machado, N.; Melamed, S.; Murray, J.; Petroff, A.; Winsborough, C. Biochar mitigates negative effects of salt additions on two herbaceous plant species. *J. Environ. Manage.* **2013**, *129*, 62−68, DOI: 10.1016/j.jenvman.2013.05.057.

(14) Chan, K. Y.; Van Zwieten, L.; Meszaros, I.; Downie, A.; Joseph, S. Agronomic values of greenwaste biochar as a soil amendment. *Soil Res.* **2007**, *45* (8), 629−634, DOI: 10.1071/SR07109.

(15) Steinbeiss, S.; Gleixner, G.; Antonietti, M. Effect of biochar amendment on soil carbon balance and soil microbial activity. *Soil Biol. Biochem.* **2009**, *41* (6), 1301−1310, DOI: 10.1016/j.soilbio.2009.03.016.

(16) Novak, J. M.; Busscher, W. J.; Laird, D. L.; Ahmedna, M.; Watts, D. W.; Niandou, M. A. S. Impact of biochar amendment on fertility of a southeastern coastal plain soil. *Soil Sci.* **2009**, *174* (2), 105−112, DOI: 10.1097/SS.0b013e3181981d9a.

(17) Zimmerman, A. R.; Gao, B.; Ahn, M.-Y. Positive and negative carbon mineralization priming effects among a variety of biochar-amended soils. *Soil Biol. Biochem.* **2011**, *43* (6), 1169−1179, DOI: 10.1016/j.soilbio.2011.02.005.

(18) McClellan, T.; Deenik, J.; Uehara, G.; Antal, M. Effects of flashed carbonized macadamia nutshell charcoal on plant growth and soil chemical properties. *Am. Chem. Soc. Agron. Abstr.* **2007**.

(19) McLaughlin, H.; Anderson, P. S.; Shields F. E.; Reed, T. B. All biochars are not created equal, and how to tell them apart. *Proceedings, North American Biochar Conference, Boulder, Colorado*, 2009; www.biochar-international.org/sites/default/files/All-Biochars--Version2--Oct2009.pdf.

(20) McBeath, A. V.; Smernik, R. J. Variation in the degree of aromatic condensation of chars. *Org. Geochem.* **2009**, *40* (12), 1161−1168, DOI: 10.1016/j.orggeochem.2009.09.006.

(21) Cao, X.; Harris, W. Properties of dairy-manure-derived biochar pertinent to its potential use in remediation. *Bioresour. Technol.* **2010**, *101* (14), 5222−5228, DOI: 10.1016/j.biortech.2010.02.052.

(22) Knicker, H. Pyrogenic organic matter in soil: its origin and occurrence, its chemistry and survival in soil environments. *Quatern, Int.* **2011**, *243* (2), 251−263, DOI: 10.1016/j.quaint.2011.02.037.

(23) Schimmelpfennig, S.; Glaser, B. One step forward toward characterization: some important material properties to distinguish biochars. *J. Environ. Qual.* **2012**, *41*, 1001−1013, DOI: 10.2134/jeq2011.0146.

(24) Wiedner, K.; Naisse, C.; Rumpel, C.; Pozzi, A.; Wieczorek, P.; Glaser, B. Chemical modification of biomass residues during hydrothermal carbonization − what makes the difference, temperature or feedstock? *Org. Geochem.* **2013**, *54*, 91−100, DOI: 10.1016/j.orggeochem.2012.10.006.

(25) Zhao, L.; Cao, X.; Mašek, O.; Zimmerman, A. Heterogeneity of biochar properties as a function of feedstock sources and production temperatures. *J. Hazard. Mater.* **2013**, *256−257*, 1−9, DOI: 10.1016/j.jhazmat.2013.04.015.

(26) Conte, P.; Marsala, V.; De Pasquale, C.; Bubici, S.; Valagussa, M.; Pozzi, A.; Alonzo, G. Nature of water-biochar interface interactions. *GCB Bioenergy* **2013**, *5* (2), 116−121, DOI: 10.1111/gcbb.12009.
(27) Sing, K. The use of nitrogen adsorption for the characterization of porous materials. *Colloid Surf. A* **2001**, *187−188*, 3−9, DOI: 10.1016/S0927-7757(01)00612-4.
(28) Dunn, K. J.; Bergman, D. J.; Latorraca, G. A. *Handbook of Geographic Exploration−Seismic Exploration: Nuclear Magnetic Resonance Petrophysical and Logging Applications*; Elsevier Science: Oxford, UK, 2002.
(29) Conte, P.; Alonzo, G. Environmental NMR: fast-field-cycling relaxometry. *eMagRes* **2013**, 389−398, DOI: 10.1002/9780470034590.emrstm1330.
(30) Kimmich, R.; Anoardo, E. Fast-field-cycling NMR relaxometry. *Prog. Nucl. Magn. Reson. Spectrosc.* **2004**, *44*, 257−320, DOI: 10.1016/j.pnmrs.2004.03.002.
(31) Morozova-Roche, L. A.; Jones, J. A.; Noppe, W.; Dobson, C. M. Independent nucleation and heterogeneous assembly of structure during folding of equine lysozyme. *J. Mol. Biol.* **1999**, *289* (4), 1055−1073, DOI: 10.1006/jmbi.1999.2741.
(32) Borgia, G. C.; Brown, R. J. S.; Fantazzini, P. Uniform-penalty inversion of multiexponential decay data. *J. Magn. Reson.* **1998**, *132* (1), 65−77, DOI: 10.1006/jmre.1998.1387.
(33) Borgia, G. C.; Brown, R. J. S.; Fantazzini, P. Uniform-penalty inversion of multiexponential decay data: II. Data spacing, T_2 data, systematic data errors, and diagnostics. *J. Magn. Reson.* **2000**, *147* (2), 273−285, DOI: 10.1006/jmre.2000.2197.
(34) Almendros, G.; Martinez, A. T.; Gonzalez, A. E.; Gonzalez-Vila, F. J.; Fruend, R.; Luedemann, H.-D. CPMAS ^{13}C NMR study of lignin preparations from wheat straw transformed by five lignocellulose-degrading fungi. *J. Agric. Food Chem.* **1992**, *40* (7), 1297−1302, DOI: 10.1021/jf00019a043.
(35) Callaghan, P. T.; Coy, A. PGSE NMR and molecular translational motion in porous media. In *Nuclear Magnetic Resonance Probes of Molecula Dynamics*; Tycho, R., Ed.; Kluwer Academic Publishers: Dordrecht, The Netherlands, 1994; pp 551.
(36) Godward, J.; Gunning, P.; Hills, B. P. An NMR protocol for determining ice crystal size distributions during freezing and pore size distributions during freeze-drying. *Appl. Magn. Reson.* **1999**, *17* (4), 537−556, DOI: 10.1007/BF03162085.
(37) Browenstein, K. R.; Tarr, C. E. Importance of classical diffusion in NMR studies of water in biological cells. *Phys. Rev. A* **1979**, *19* (6), 2446−2454, DOI: 10.1103/PhysRevA.19.2446.
(38) Laudicina, V. A.; De Pasquale, C.; Conte, P.; Badalucco, L.; Alonzo, G.; Palazzolo, E. Effects of afforestation with four unmixed plant species on the soil−water interactions in a semiarid Mediterranean region (Sicily, Italy). *J. Soil Sediment* **2012**, *12* (8), 1222−1230, DOI: 10.1007/s11368-012-0522-0.
(39) Stingaciu, L. R.; Pohlmeier, A.; Blümler, P.; Weihermüller, L.; van Dusschoten, D.; Stapf, S.; Vereecken, H. Characterization of unsaturated porous media by high-field and low-field NMR relaxometry. *Water Resour. Res.* **2009**, *45* (8), DOI: 10.1029/2008WR007459.
(40) Korb, J.-P. Surface diffusion of liquids in disordered nanopores and materials: a field cycling relaxometry approach. In *Fluid Transport in Nanoporous Materials*; Conner, W. C., Fraissard, J., Eds.; Academic Press, Springer: Dordrecht, The Netherlands, 2006.
(41) Bakhmutov, V. I. Front matter. In *Practical NMR Relaxation for Chemists*; Wiley: Chichester, UK, 2004.